Behavior of Cumulus Activity and the Structures of Circulations in an "Aqua Planet" Model

Part I: The Structure of the Super Clusters

By Atusi Numaguti and Yoshi-Yuki Hayashi

Department of Earth and Planetary Physics, University of Tokyo, Tokyo 113, Japan
(Manuscript received 12 December 1990, in revised form 31 July 1991)

Abstract

As an extension of the 'aqua planet' experiments by Hayashi and Sumi (1986, HS86), GCM experiments with various SST distributions and cumulus parameterizations are performed in order to examine the structure of cumulus activity and its parameter dependence. In part I, the results of the analyses concentrating on the super clusters are described.

The super clusters, which were named by HS86, are expressed in the model as continuously moving precipitating areas of the grid scale. The associated circulation structure can be explained in terms of the wave-CISK dynamics of Kelvin waves. The super clusters become more active when a warmer SST is used. On the other hand, the 30 day oscillation, that is an eastward-moving planetary scale structure, is more distinct when a colder SST is used.

The behavior of cumulus activity is highly sensitive to the choice of cumulus parameterization. When the moist convective adjustment scheme is used instead of Kuo's (1974) scheme, the eastward-moving structure of the grid scale is no longer observed at the equator. However, the planetary scale structure still clearly appears in the experiment with the moist convective adjustment scheme.

1. Introduction

1.1 The experiments of Hayashi and Sumi (1986)

Recently, a number of experiments with general circulation models (GCMs) were performed in order to reveal the relationship between tropical circulation and cumulus activity. Among others, the results of Hayashi and Sumi (1986, called HS86 hereafter) are very informative for the purpose of revealing systematic behaviors of cumulus activity. Their GCM experiments were carried out under simple and idealistic conditions in order to separate the essential dynamics from the complexity caused by the boundary conditions of the real world. The condition they used is that the whole earth surface is covered by the 'ocean', which means a completely wet surface with a prescribed temperature distribution. The sea surface temperature (SST) is specified to be uniform with longitude and symmetric between the hemispheres. The cumulus activity in the GCM is expressed on each grid point in terms of a moisture sink, *i.e.*, precipitation, latent heat source, and vertical redistribution of moisture and sensible heat. The amount of precipitation can be regarded as an index of cumulus activity in the model tropics.

Concentrating on the time-space distribution of precipitation in the tropics, the results of HS86 are summarized as follows:

(1) The latitudinal distribution of the time-averaged precipitation has two peaks at around 10 degrees of the both hemispheres, although the prescribed SST distribution has only one peak at the equator.

(2) There are several precipitating areas on the synoptic scale[1] at the equator. They move continuously eastward and travel around the equatorial circle in about 30 days.

(3) Such precipitating areas are not distributed uniformly in the longitudinal direction. There is a modulation of precipitation amount by planetary scale structures, especially a structure of wavenumber one. This modulation structure also moves eastward at the same speed as individual precipitating areas. In the field of zonal wind,

[1] The term 'synoptic scale' may be rather ambiguous. Here we use this term as referring to the scale which is one order smaller than the 'planetary scale' that is comparable to the entire latitudinal circle.

there appears the more significant signal of wavenumber one.

There seem to exist certain phenomena in the real atmosphere corresponding to the three features listed above. We will refer to the first feature as 'double ITCZs' (inter tropical convergence zones). In the real world, the ITCZ, which is characterized by large low-level convergence and high cumulus activity, is rarely located at the equator. It usually exists off the equator, and sometimes two ITCZs coexist on the both sides of the equator (Hubert *et al.*, 1969).

The second feature, that is, the synoptic scale precipitating area moving eastward continuously at the equator is called a 'super cluster' by HS86. In the real atmosphere, eastward movement of cloud regions on the synoptic scale has been recognized (Nakazawa, 1988; Hayashi and Nakazawa, 1989). Nakazawa (1988), for instance, found eastward-moving signals with the scale of about 3000 km from OLR (outgoing longwave radiation) data. Since the super clusters in HS86's model seem to correspond to those phenomena in the real tropics, the cloud regions observed in the real atmosphere are also called 'super clusters' or 'super cloud clusters'.

HS86 regarded the third feature as the model counterpart of the 30 to 60 day oscillation or the Madden-Julian oscillation (Madden and Julian, 1972, referred to as MJ oscillation hereafter) in the tropical atmosphere. The structure of the circulation simulated in the model is in good agreement with the structure of the MJ oscillation (*e.g.*, Murakami *et al.*, 1984).

These results indicate that a hierarchical structure of cumulus activity forms spontaneously in the tropical atmosphere even if the boundary conditions are uniform. Super clusters exist as a fine structure inside of the MJ oscillation. In the real tropics, there are so-called cloud clusters inside of the super clusters (Nakazawa, 1988), although they are out of the resolution limit and cannot be realized in the model.

1.2 Questionable points in HS86's results

From the results summarized above, it may be said that HS86 succeeded in describing some basic features of cumulus activity coupled with large scale dynamics. However, there remain some questionable points.

The first point is the disagreement with other GCM studies. Several 'aqua planet' type GCM experiments have been performed since HS86, and the results are not in accord with each other (Lau *et al.*, 1988; Swinbank *et al.*, 1988; Tokioka *et al.*, 1988). Lau *et al.* (1988) obtained a planetary scale structure which moves eastward with a period of about 30 days. However, the zonal mean precipitation pattern has a single peak at the equator: A double ITCZ structure does not appear in their result. Moreover, continuous movement of synoptic scale disturbances cannot be found in the sequence of precipitation. Swinbank *et al.* (1988) also succeeded in simulating an eastward-moving planetary scale disturbance which has a period of around 30 days. Their results show a double ITCZ structure. However, they did not describe the existence of super clusters. In the experiments of Tokioka *et al.* (1988), an eastward-moving structure of planetary scale with a 30 to 40 day period also emerges, but we cannot see the double ITCZ structure in their results (Ose *et al.*, 1989). From a comparison among these results, it can be said that all the GCM experiments commonly succeed in simulating the MJ oscillation. For the double ITCZ structure, the results diverge from each other. Moreover, there are no other GCM studies than HS86 in which the existence of super clusters is clearly pointed out. As is often stated in the literature, the present status of GCMs is far from perfect. Especially, the adequacy of the parameterization of cumulus convection is highly questionable. In the GCM experiments listed above, different parameterizations of cumulus convection are used. It may be possible that the variety of these results is caused by the difference of parameterization.

The second point is the limitation of the model resolution. The horizontal scale of super clusters approximately corresponds to the smallest resolvable scale in the model of HS86. Therefore, it is rather questionable whether the super cluster in the model is a physically meaningful structure or not.

The third point is the incompleteness of description. There is a remarkable feature of cumulus activity in the actual tropics which HS86 never referred to. That is the easterly wave disturbance, which is a wavy disturbance of 1000 km scale that moves westward through the non-equatorial ITCZ regions (Reed and Recker, 1971).

1.3 Theoretical concepts of interaction of cumulus and large scale circulations, and their application to tropical disturbances

In this paper, with these questionable points in mind, we will reproduce HS86's experiments and describe the structures of precipitation and associated circulations. Before describing the results, we will briefly summarize some important concepts of generation and maintenance of combined structures of cumulus activity and large scale circulations in order to avoid confusion in the later description.

In general, some sort of energy supply is necessary for generation and maintenance of finite amplitude disturbances against dissipative processes. In the tropics, energy supply to disturbances through heating associated with latent heat release is important. The existence of disturbances affects the distribution of heating by some processes. When the distri-

bution of heating works in the sense of reinforcing the pre-existing disturbances, a self-sustained disturbance may exist. Note that the correlation between the distributions of heating and temperature must be positive for the disturbances to be reinforced.

The heating associated with latent heat release is mainly achieved in the form of cumuli by the ascent and condensation of moist air originated from the boundary layer. Fluctuations of heating are caused by fluctuations of facility for cumuli to emerge and fluctuations of energy (moist static energy) contained in the air at the boundary layer to be supplied to cumuli.

A typical process associated with large scale disturbances which modifies the facility for cumuli to emerge is the existence of upward motion. It is generally believed that the stratification of the tropical atmosphere is conditionally unstable. However, this instability is potential: Development of cumuli is suppressed by the existence of a stable layer at the top of the boundary layer and/or by the dryness of the free atmosphere. Existence of upward motion in the lower levels may relax the suppression and cumuli may develop. This upward motion also causes moisture convergence and brings a further suitable condition for the endurance of cumulus activity. A large scale disturbance can be intensified, when the modification of the distribution of heating with upward motion associated with the disturbance occurs consistently. This mechanism of intensification is usually called 'CISK' (conditional instability of second kind).

Suppose that there is a vortex which has a warm core in the middle layer. In the lower layer, the pressure of the center is low and there is an upward motion caused by frictional convergence. In this case, the disturbance will grow if the heating is intensified by this upward motion. This mechanism is proposed as an explanation of development and maintenance of vortex-like disturbances such as hurricanes (Charney and Eliassen, 1964). When a wave-like disturbance is present, there is also a possibility of intensification by frictional convergence. Wang (1988) pointed out that, in the case of an equatorial Kelvin wave, there is an area of frictional convergence to the east of the upward motion. He showed that the Kelvin wave is unstable in a linear theory if the enhancement of heating by this frictional convergence is incorporated. In this paper, we will use the term 'frictional CISK' in referring to the process in which disturbances, whether vortices or waves, are intensified through frictional convergence in the boundary layer.

As for wave-like large scale disturbances, the CISK mechanism can be considered even if the frictional effect is neglected, because of the existence of intrinsic vertical motion associated with them. This intensification mechanism is proposed as an explanation of tropical wave disturbances and called 'wave-CISK'. Hayashi (1970) and Lindzen (1974) showed that, when the heating at all levels is assumed to be proportional to upward motion at a certain height (especially at a low level), the wave may be unstable in a linear sense. Here, this assumption is called 'wave-CISK parameterization'. As emphasized before, the phase relationship that the correlation between temperature and heating is positive must be maintained in growing disturbances. However, if we simply assume that the heating is proportional to upward motion at each level, the resultant modes are only non-propagating convective motions or neutral waves with 'reduced gravity effect' (Gill, 1982). The heating never intensifies propagating waves because the phases of upward motion and temperature are in quadrature (Bolton, 1980). If the wave-CISK parameterization is used, on the other hand, propagating unstable modes are enabled by a shift of the phases caused by a slant of phase structure of the wave in the longitudinal-vertical plane. It can be interpreted that the unstable modes are formed by the coupling of two neutral vertical modes (Chang and Lim, 1988). In this paper, we will use the term 'wave-CISK' in referring to the process that intensifies wave disturbances through the coupling between vertical motion of wave and cumulus activity, which is typically represented by the wave-CISK parameterization.

A typical process associated with large scale disturbance which modifies the energy contained in the air at the boundary layer is a change of surface energy fluxes. The latent heat flux due to surface evaporation is dominant in surface energy fluxes in the tropical oceanic region. Evaporation rate from the sea surface, which is given by Eq. (1), is large when the surface wind speed is large.

$$E = \rho C_D |v| (q^* - q_a), \tag{1}$$

where ρ is air density, C_D bulk coefficient, $|v|$ wind speed near the surface, q^* saturation specific humidity at the surface, and q_a is specific humidity of air near the surface. When a large scale disturbance exists, it modifies the evaporation rate through change of surface wind speed, and accordingly modifies the energy contained in the air at the boundary layer. The disturbance can be intensified through the resultant modification of heating. Suppose that there is a vortex with a warm core over the ocean. The wind blows strongly near the center of the vortex and the moisture supply is large near the center. The disturbance will be intensified if the modification of heating effectively increases the temperature of the warm core. This process is considered to be important for intensification and maintenance of hurricanes (Emanuel, 1986). Emanuel (1987) and Neelin *et al.* (1987) also showed that

this process allows the existence of linearly unstable eastward-propagating waves in the equatorial region. In the presence of mean easterly wind, the surface wind speed is large in the warm easterly region to the east of the upward motion, while it is small in the cool westerly region to the west. Thus large evaporation and hence large heating occurs in the warm sector. In this paper, we will use the term 'evaporation–wind feedback' in referring to such a process, whether in regard to vortices or waves.

Some recent studies (*e.g.*, Xu and Emanuel, 1989) pointed out that the stratification in the tropical atmosphere is very close to the moist neutral stratification if the effect of loading water condensate is taken into account. If the stratification is exactly restricted to the moist adiabat everywhere, the thermal structure of the atmosphere is completely determined by the thermal state of the boundary layer air. In this case, temperature change will be caused only by the change of energy contained in the air of boundary layer and never be caused by the change of the facility of emergence of cumuli. No CISK (frictional CISK and wave-CISK) mechanisms can work in such a situation. With these assumptions for the stratification, Emanuel (1987) emphasized the importance of an intensification mechanism of disturbance through the change of the energy contained in the air of the boundary layer, especially evaporation–wind feedback. However, it has never been discussed quantitatively to what extent the stratification should follow the moist adiabat in order to accept the argument of Emanuel (1987) and to reject the possibility of CISK.

1.4 Aim of this paper

As stated before, there are some observational studies that suggest the existence of a hierarchical structure composed of super clusters and the MJ oscillation. On the other hand, no model studies other than HS86's clearly show such a hierarchical structure. In this paper, in order to get more detailed information on the hierarchical structure obtained by HS86, we will reproduce HS86's experiments and describe the structures of disturbances in the model.

The most remarkable result of HS86's experiments is the presence of super clusters as a fine structure inside the MJ oscillation. Formerly, there were few studies that indicated the existence of such features in the real atmosphere (Zangvil, 1975). It was only recently that the existence of super clusters came to public notice. Thus, the number of corresponding theoretical studies is very small. Lau and Peng (1987) showed an eastward movement of synoptic scale precipitating areas using a rather simple nonlinear wave-CISK model. In their model, however, only one precipitating area exists at the center of the planetary scale circulation, which differs from the planetary scale modulation of multiple super clusters shown in HS86. As a dynamical description of the super clusters, HS86 considered that the super cluster in their model is a mode in which a Kelvin wave and a Rossby wave are coupled through cumulus heating. However, the actual feature is not clear because they did not analyze their results in this context.

Bearing these situation in mind, the results of the model experiments, which are the extended version of HS86's, are analyzed in Part I of this paper, concentrating on the synoptic scale structures around the equator. The results concerning the planetary scale structures and the structures off the equator will be described in Part II (Numaguti and Hayashi, 1991). The description of the model and the experiments will be presented in Section 2. In Section 3, behavior of precipitating areas will be described and the characteristics indicated by HS86 will be confirmed. The parameter dependence of the behaviors will be also described. We will examine the structure of the circulations accompanied by the precipitating areas, with the aid of the composite method. The results will be described in Section 4. Another experiment using the moist convective adjustment scheme instead of Kuo's scheme is performed to determine the dependence on cumulus parameterization. The results will be presented in Section 5, and compared with the results in Sections 3 and 4. Discussion on the results is presented in Section 6. The Appendix describes a simple linear model which explains the structures of circulations associated with super clusters.

2. The model and experiments

The model used in this study is a global spectral model originally developed by the Japan Meteorological Agency (Kanamitsu *et al.*, 1983), which is virtually the same model used by HS86. The horizontal resolution is triangular 42 and the physical processes are calculated at grid points located at approximately every 2.8 degrees. The model has 12 levels in the vertical direction. There are 4 levels in the planetary boundary layer, while there are only two levels in the stratosphere. The parameterization of the radiative process is based on Katayama (1972) and calculated every 3 hours. The cloud amount is diagnosed through relative humidity. A simple vertical diffusivity estimated from bulk Richardson number is utilized for the parameterization of the boundary layer processes.

Since the parameterization of cumulus convection is essential for the purpose of this study, we will describe them rather in detail. In the first three experiments (see Table 1), the parameterization of Kuo (1974), which is the same as HS86 used, is adopted. The essentials of the parameterization are as follows. Heating and redistribution of moisture, which are proportional to moisture convergence I, occur in

Table 1. The setup of the experiments

Exp.	SST	cumulus parameterization
K1	standard(HS86)	Kuo (1974)
K2	+2K	Kuo (1974)
K3	−2K	Kuo (1974)
A1	standard	moist convective adjustment

the cloud layer when the following three conditions are satisfied.

- A moist unstable layer exists beyond the planetary boundary layer.
- The moisture convergence integrated in the cloud layer I is positive.
- The averaged relative humidity in the cloud layer is larger than a certain critical value r_C.

Here, the lower boundary of the cloud layer is defined as the lowest level of the moist unstable layer beyond the planetary boundary layer. The upper bound of the cloud layer is defined as the level where a saturated parcel, which moves up moist-adiabatically from the lower boundary, loses its buoyancy. The vertical distribution of heating is estimated to be proportional to the difference of temperature between this parcel and the environment. The vertical distribution of moistening is also estimated to be proportional to the difference of specific humidity. The effect of entrainment is not accounted in the calculation of temperature and humidity of the parcel. The value of 0.9 is adopted as r_C. The β value, which is the ratio of moisture to be used for moistening to converged moisture, is formulated as a function of vertically averaged relative humidity $\bar{r}$. It is 1 for $\bar{r} \leq 0.9$, 0 for $\bar{r} \geq 0.91$, and is linearly dependent on $\bar{r}$ between.

In the other experiment, the moist convective adjustment scheme (Manabe *et al.*, 1965) is adopted as the cumulus parameterization. In this parameterization, the stratification is adjusted to be neutral to moist adiabatic processes instantaneously whenever the following two conditions are satisfied.

- A moist unstable layer exists.
- The relative humidity in the cloud layer is larger than a certain critical value r'_C.

In this scheme, the cloud layer is defined as the moist unstable layer. When the upper layer becomes unstable through the adjustment of the lower layer, the scheme is applied iteratively. The value of 1.0 is adopted as r'_C. The moist convective adjustment scheme does not require moisture convergence explicitly.

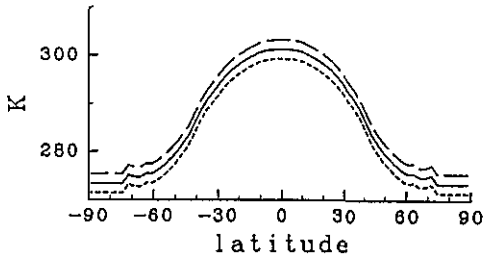

Fig. 1. Distributions of the sea surface temperature (SST) used in the experiments (Unit; K). Solid line; standard experiment K1 and moist convective adjustment experiment A1. Broken line; high SST experiment K2. Dotted line; low SST experiment K3.

2.2 Setup of experiments

Four series of time integrations are performed. The basic parameters of the experiments are the same as HS86. The whole surface is covered with an 'ocean', in which the value of SST is prescribed as a function of latitude only and completely wetted. The surface albedo is taken to be longitudinally uniform. The location of the sun is fixed at the equinox and no seasonal variation is allowed, though the diurnal variation is included.

The setup of the experiments is summarized in Table 1. The SST distributions are shown in Fig. 1. They are hemispherically symmetric and zonally uniform with a peak at the equator. The SST distribution for the standard experiment (K1) is the same as HS86's. The SST is increased by 2K everywhere in experiment K2, whereas the SST is decreased by 2K everywhere in experiment K3. Experiment A1 is the same as experiment K1 except for the difference of cumulus parameterization.

The time integration is performed in the following way. The spin-up run is performed for 150 days in the condition of K1 using the zonal mean of the final result of HS86 as the initial condition. The result of the spin-up run is used as the initial condition for each experiment. In each experiment, the model is integrated for 120 days, and the data of last 60 days are used for analyses. We refer to the first day of this period of analyses as 'day 0'. The data is sampled every 6 hours. In the following analyses, the original model vertical coordinate $\sigma (=p/p_s$, p is

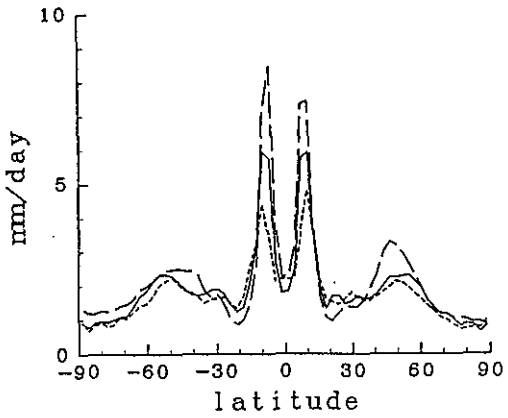

Fig. 2. Latitudinal distributions of time and zonal mean precipitation (Unit; mm/day). Solid line; standard experiment K1. Broken line; high SST experiment K2. Dotted line; low SST experiment K3.

pressure, p_s is surface pressure) is utilized instead of the conventional pressure coordinate.

3. Distribution of precipitation

In this section, some important characteristic features of the distribution of precipitation in the experiments with Kuo's cumulus parameterization (K1 ~K3) are described.

3.1 Latitudinal distribution of precipitation

In Fig. 2, the latitudinal distributions of precipitation averaged by time and longitude are shown for the three experiments. The result of the standard experiment K1 displays a double ITCZ structure which has two peaks around 10 degrees latitudes, as stated in HS86. The double ITCZ structure exists in all experiments regardless of the value of SST. Comparing the results of the three experiments, the peak value is the larger with the higher SST. Note that the precipitation amount at the equator is approximately the same in the three experiments.

3.2 Longitude-time distribution of precipitation at the equator

Figure 3 shows the longitude–time section of precipitation within a latitudinal band of 6 degree width centered at the equator. The results of the standard experiment K1 reproduce the HS86's results (see Fig. 2 in HS86), which are characterized by the continuous eastward movement of the synoptic scale precipitating areas and their modulation on a planetary scale. It takes about 38 days to encircle the equator both for the synoptic scale structure and the planetary scale structure, which means the speed of movement is about 12 m/s.

Here we have to note that the longitudinal scale of the synoptic scale precipitating area is smaller than that described by HS86. The reason is the difference in the sampling time. HS86 used the 12hour

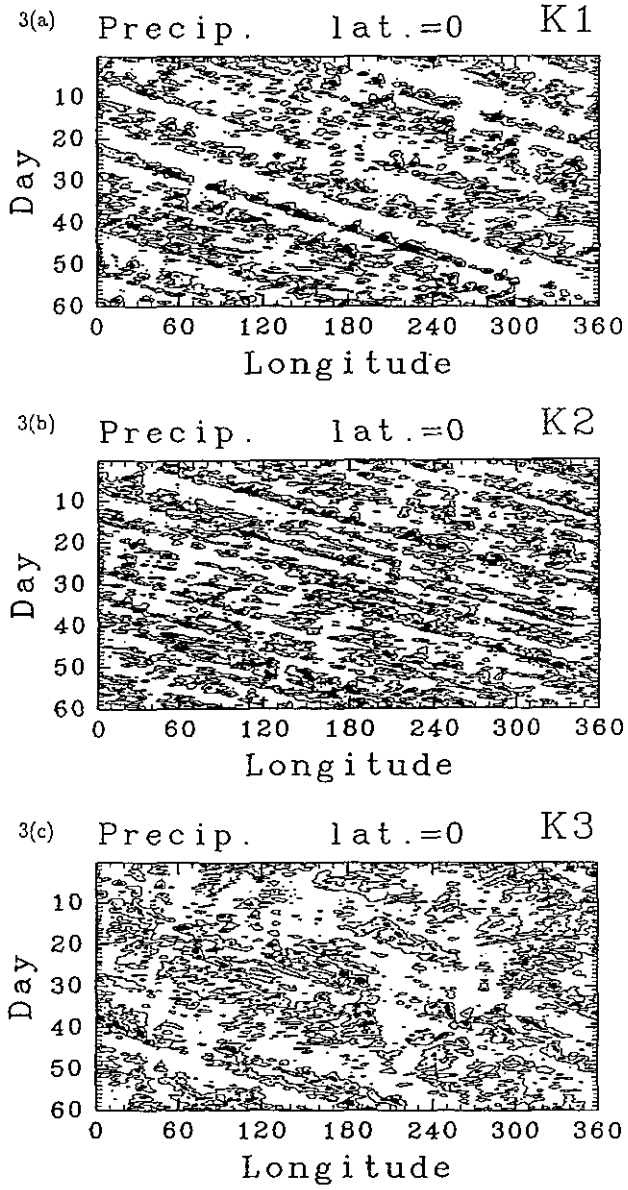

Fig. 3. Longitude–time distributions of precipitation at the equator. Contours indicate 2 mm/day and areas of over 10 mm/day are shaded. (a) Standard experiment K1, (b) high SST experiment K2, (c) low SST experiment K3.

cumulative precipitation value, while we used the 6hour cumulative value. HS86 overestimated the longitudinal scale of the moving areas. An examination of the values at every model time step shows that the precipitation occurs within 1 to 3 grid points (not shown in figures). This corresponds to the smallest resolvable scale in the spectral model. The super clusters in the model are expressed as continuously moving precipitating areas on the *grid scale*. On the other hand, the scale of super clusters in the real atmosphere is estimated to be about 3000 km from OLR data (Nakazawa, 1988). The correspondence of the horizontal scale between the super

clusters in the model and those in the nature is not so good as that stated by HS86. Thus, in order to avoid confusion, we use the word 'grid scale[2] precipitating area' rather than 'super cluster' when we describe the results of the model afterwards. Similarly, we use the word 'planetary scale (modulation) structure' instead of 'MJ oscillation'. Another difference between our results and HS86's is that the planetary scale structure in our Fig. 3a is not so clear as in HS86's figure. Examination of the result of the long time range integration (not shown) suggests that the amplitude of the planetary scale structure fluctuates considerably.

For the high SST experiment K2, the grid scale precipitating areas exist more clearly and move more continuously than in K1. The number of precipitating area within the equatorial belt is larger in K2 than in K1. On the other hand, the planetary scale modulation structure is hardly seen. It takes about 35 days to encircle the equator, that is, the speed of movement is about 13 m/s.

The results of the low SST experiment K3 are opposite in nature to K2. The grid scale eastward-moving precipitating area becomes rather unclear, whereas the planetary scale structure, especially the structure of wavenumber 1 to 2, becomes more prominent than in K1. The grid scale precipitating areas are concentrated in the region with the longitudinal extent of 10000 km (for example, 60 degrees to 180 degrees at day 20 in Fig. 3c). To the west of the region of intense precipitation, regions of rather weak and irregular precipitation exist (for example, 0 degrees to 60 degrees longitude at day 20). It takes about 47 days to encircle the equator, that is, the speed of movement is about 10 m/s.

In all experiments, the difference in speed between the grid scale structure and the planetary scale structure is not recognized. Note that the speed of eastward movement increases as SST increases.

4. Analyses of the circulation structures associated with the precipitating areas

In this section, the structure of circulations associated with the precipitating areas is examined by the use of composite analyses, to discuss the behavior of precipitating areas described in the previous section.

4.1 Structure of mean fields

Figure 4a is the distribution of the zonal mean vertical motion field in experiment K1. Corresponding to the maximum of precipitation, the maximum of upward motion is located off the equator. There is a weak downward motion at the equator centered around 300 mb. Figure 4b shows the stream function of the meridional circulation. An 'indirect' circulation exists in the equatorial upper troposphere. The mean zonal wind field has a strong easterly jet around the equator as shown in Fig. 4c.

This peak value of −13 m/s is approximately the same as that realized by an air parcel which is initially placed at rest at 10 degree latitude and

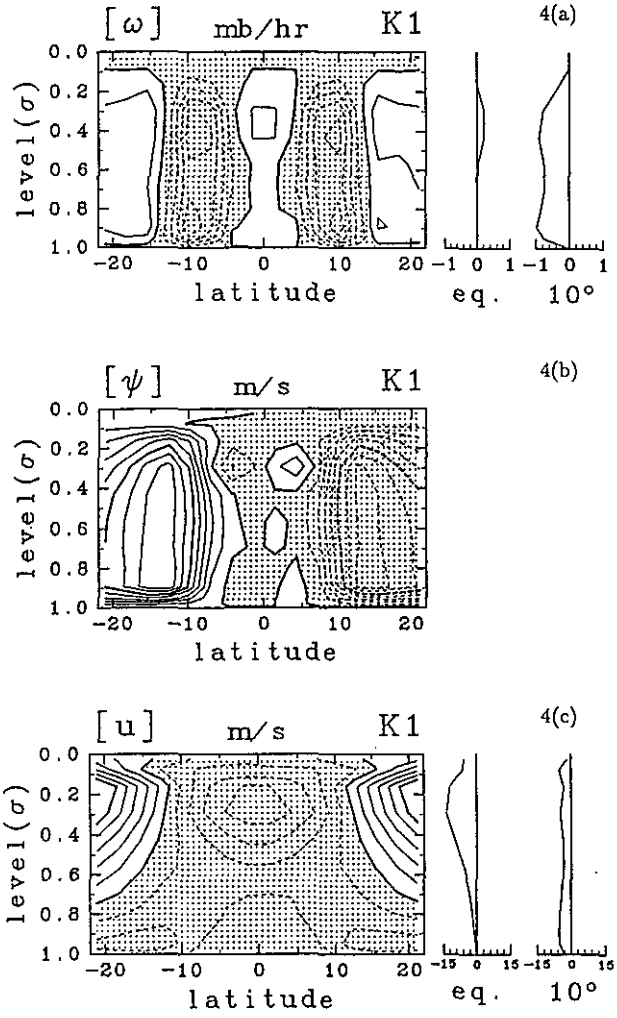

Fig. 4. Zonal and time mean distributions of the circulation field in experiment K1. The plots on the right side indicate the values at the equator and 10 degrees latitude. (a) Vertical p-velocity $[\omega]$. The contour interval is 0.2 mb/hr and areas of upward motion are shaded. (b) Meridional stream function $[\psi]$. The contour interval is 0.02 m/s and negative areas are shaded. Definition of $[\psi]$ is

$$[\dot{\sigma}] = \frac{1}{a}\frac{\partial[\psi]}{\partial\varphi}\ , \quad [v] = -\frac{\partial[\psi]}{\partial\sigma}$$

(c) Zonal wind $[u]$. The contour interval is 3 m/s and negative areas are shaded.

[2]This words only express that the scale is nearly the smallest resolvable scale in *our* model. We do not explore whether the structure on the grid scale still appears if the resolution of the model is increased.

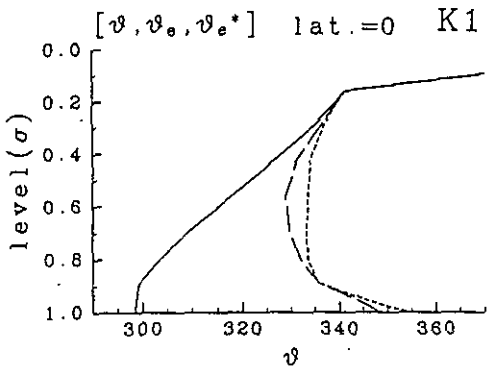

Fig. 5. Vertical structures of time and zonal mean temperature field at the equator in experiment K1 (Unit; K). Solid line; potential temperature. Broken line; equivalent potential temperature. Dotted line; saturated equivalent potential temperature.

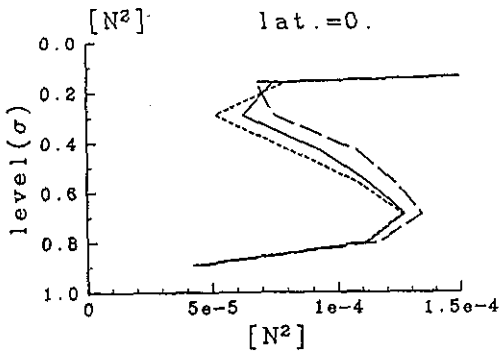

Fig. 6. Vertical distributions of static stability N^2 at the equator of time and zonal mean (Unit; s^{-2}). Solid line; standard experiment K1. Broken line; high SST experiment K2. Dotted line; low SST experiment K3.

moves to the equator with its angular momentum conserved. The absolute vorticity in the upper troposphere is almost zero around the tropical region within 10 degree latitudes of both hemisphere. Actually, when the upward motion is concentrated at a certain latitude and the transport of angular momentum is assumed to be dominated by the mean meridional circulation, the zonally averaged angular momentum in the tropical upper troposphere is expected to have approximately the same value as that of the planetary angular momentum at the latitude of the upward motion (Held and Hou, 1980). The zonally averaged angular momentum $[M]$ is expressed as:

$$[M] = \Omega a^2 \cos^2\varphi + [u] a \cos\varphi \ , \qquad (2)$$

where u is the zonal velocity, φ the latitude, Ω the angular velocity of the rotation of the earth and a is the radius of the earth. [ ] represents the zonal mean whereas ( )* represents the deviation from zonal mean: This convention is also used in the title of the figures. Since the following relationship holds between the zonally averaged angular momentum and absolute vorticity $(f + [\zeta])$, the latter will be zero if the former is uniform in latitude.

$$\frac{1}{a^2\cos\varphi}\frac{\partial [M]}{\partial \varphi} = -2\Omega\sin\varphi + \frac{1}{a\cos\varphi}\frac{\partial}{\partial\varphi}([u]\cos\varphi)$$
$$= -(f + [\zeta]) \ , \qquad (3)$$

The fact that the mean vorticity field of the lower troposphere is greatly different from that of the upper troposphere will have considerable influence on the structure of disturbances.

Figure 5 shows the vertical stratification at the equator. It agrees with the standard stratification of the real tropics (Yanai *et al.*, 1973), in the sense that the lower layers are potentially unstable and the upper layers are stable for moist process. The vertical stratification at 10 degrees latitude is qualitatively the same as that at the equator.

The structure of mean fields is basically the same among the three experiments K1∼K3, although there are some quantitative differences. The higher SST results in stronger meridional circulation and a more significant ITCZ. The experiment with the higher SST also results in a more stable stratification (Fig. 6). These results correspond to the fact that the moist adiabatic lapse rate is small when the temperature is high and consequently the atmosphere is moister. They suggest that the tropical stratification in the model is governed by the moist adiabatic process.

4.2 The composite technique

It is considered that various 'noises' (disturbances which have no direct relationship with the structure concerned) are superimposed on the circulation field. The composite analysis using precipitation as a key is performed to exclude the noises and extract the common feature associated with the precipitating areas. The procedure is as follows.

Firstly, a reference latitude is chosen. Then we select the longitudes of precipitation peaks around the reference latitude from the data at each sampling time in the following way.

1. Apply longitudinally moving average with a rectangular averaging area.
2. Then the longitudes of peaks are selected by the following criteria:
   - The amount of precipitation at the longitude is above a certain critical value.
   - The amount of precipitation at the longitude is maximum among those at the grid points within a certain longitudinal extent centered there.

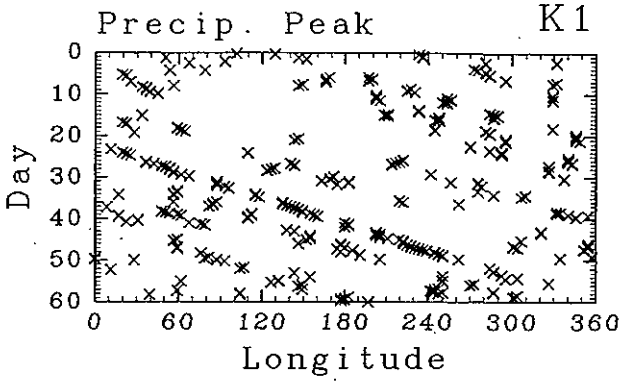

Fig. 7. Precipitation peaks in experiment K1 picked up from Fig. 3a.

The moving average is applied because a reduction of noise is expected. We chose the averaging area as 1500 km square, the critical precipitation amount as 2.5 mm/6hr and the longitudinal extent of scanning for the peak as 4000 km. Figure 7 shows the result for experiment K1 with the reference latitude at the equator. Note that the peaks in this definition do not necessarily mean the peaks in the horizontal plane or longitude-time section. After picking up the longitudes of the peaks, the data of various circulation fields are longitudinally shifted so that each longitude of the peak comes to 180 degrees, and are averaged. This is the composite with the reference to the precipitation peaks at the reference latitude.

4.3 Structure of circulation associated with the eastward-moving grid scale precipitating areas at the equator

In this subsection, the composite structure with reference to individual precipitating areas at the equator is examined. The composite is considered to reflect the structure associated with the eastward-moving grid scale precipitating areas. The characteristic feature of the composited figures described below can also be recognized in the figures of fields around a precipitating area at each instant. We mainly describe the composite structure for experiment K2, which shows the clearest eastward movement of grid scale precipitation.

Figure 8a shows the composite of precipitation. The spatial extent of precipitation appears to be

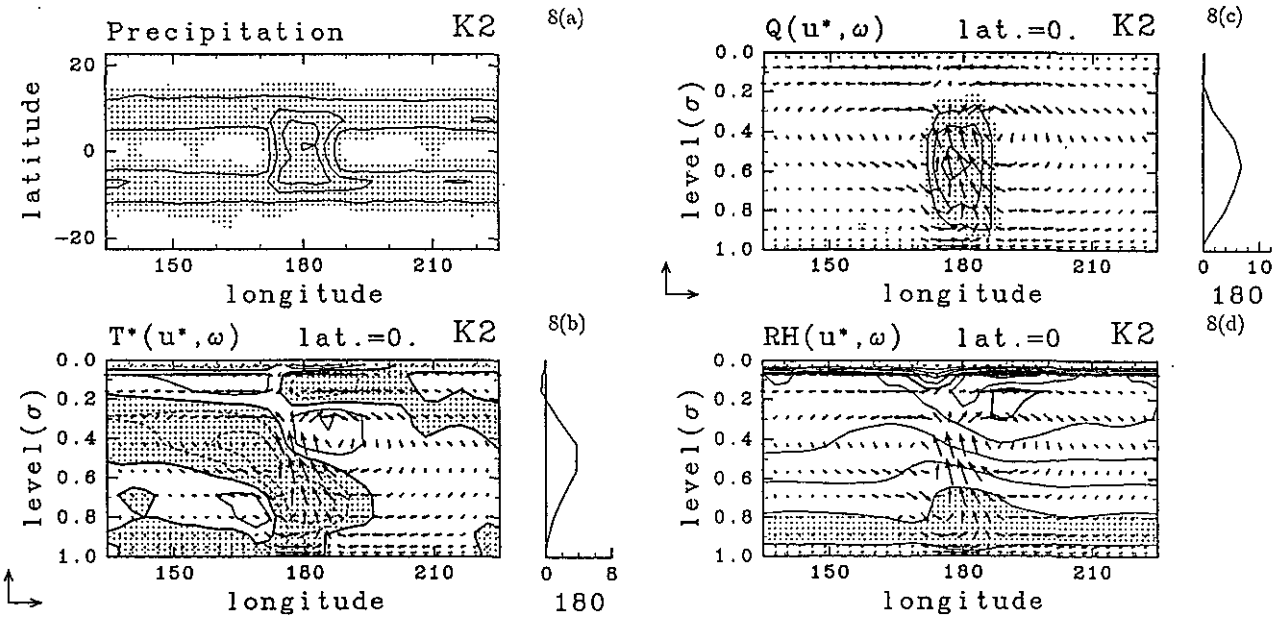

Fig. 8. Composite structures with reference to precipitation peaks at the equator in experiment K2. (a) Horizontal distribution of precipitation. The contour interval is 4 mm/day and areas of over 2 mm/day are shaded. (b) Longitude–height section of temperature (contour) and wind vectors at the equator. Zonal means are subtracted for temperature and zonal wind. The contour interval is 0.2K and negative areas are shaded. Plot on the right side is the vertical distribution of vertical p-velocity ω (Unit; mb/hr) at the precipitation peak (180 degrees longitude in the figure). (c) Longitude–height section of heating by cumulus (contour) and wind vectors at the equator. Zonal mean is subtracted for zonal wind. The contour interval is 2K/day and areas of over 1K/day are shaded. Plot on the right side is the vertical distribution of heating (Unit; K/day) at the precipitation peak. (d) longitude–height section of relative humidity (contour) and wind vectors at the equator. Zonal mean is subtracted for zonal wind. The contour interval is 10 % and areas of over 90 % are shaded. In each figure, the unit vectors shown at the left side bottom represent 5 m/s and 5 mb/hr respectively.

about 2000 km both in longitude and latitude. The amount of precipitation off the equator is large. There are areas of suppressed precipitation adjacent to the precipitating area. Figures 8b–8d represent the longitude–height sections of composite circulation. Note that the temperature and zonal wind of these figures are the deviations from the zonal mean. There is an intense updraft over the precipitation peak. The center of the low level convergence is located at about 500 km east of the precipitation peak, and the center of the upper level divergence is located rather west of the peak. The upward motion ranges from the convergence to the divergence and its axis is slanted westward. It is noteworthy that there is a rather intense localized downdraft at the 800 mb level about 1000 km west of the precipitation peak. On the other hand, no significant downdraft exists at that level to the east of the peak. Furthermore, there is a remarkably strong westerly wind below the 900 mb level over the precipitation peak. The corresponding easterly wind to the east of the peak is not so strong.

The field of temperature also shows a slantwise and asymmetric structure. In the levels higher than 500 mb, the region of positive temperature deviation exists to the east and region of negative deviation to the west. In the level around 700 mb, there is a low temperature region over the precipitation peak. On the whole, there is a high temperature region to the east of updraft and low temperature region to the west, which is consistent with the eastward propagation of the structure if the adiabatic cooling is assumed to be larger than the heating by cumulus. The existence of a high temperature region to the west of the aforementioned localized downdraft is also consistent with the propagation. There seems to be a certain structure over the tropopause, but we will not mention it here, because the resolution is not sufficient and the structure suffers from the upper boundary problem.

The field of heating by cumulus (Fig. 8c) has no slantwise structure. The peak of the heating is located around 550 mb, and the vertical profile of heating does not depend on the longitude. The relative humidity field (Fig. 8d) shows that the area around 700 mb level where the value is over 90 % is restricted to the region over the precipitating area. At the upper level, the relative humidity to the west of the precipitating area is rather high. Around 800 mb level about 1000 km west of the precipitation peak, an abrupt decrease of relative humidity is seen. The dry air seems to flow down into this region through the localized downdraft.

Figures 9a–9b represent the horizontal structures of the circulation. They show the height field $Z(\sigma) + g^{-1}RT \ln p_s$ which is the approximation of $z(p)$, and the wind field at σ surfaces. In the upper level (Fig. 9b), the structure represents the characteristics of a Kelvin wave, *i.e.*, the dominance of zonal wind, and the correspondence between easterly (westerly) wind and low (high) pressure. However, the amplitude of meridional wind is rather large near the precipitation peak and the outflow seems to be isotropic. These structures extend to about 10 degree latitudes. In the lower level (Fig. 9a), the structure to the east of the precipitation peak is not so different from that of the upper layer, while the structure to the west of the peak looks different from that of the upper level. An intense and localized westerly wind appears and the horizontal scale of structure is smaller than that of the upper layer. This structure to the west of the peak is quite different from the Rossby type response which appears in the linear steady response to a heat source (Gill, 1980). From these figures, the importance of a Rossby-wave-like response, which HS86 and Chao (1987) stated, can hardly be recognized.

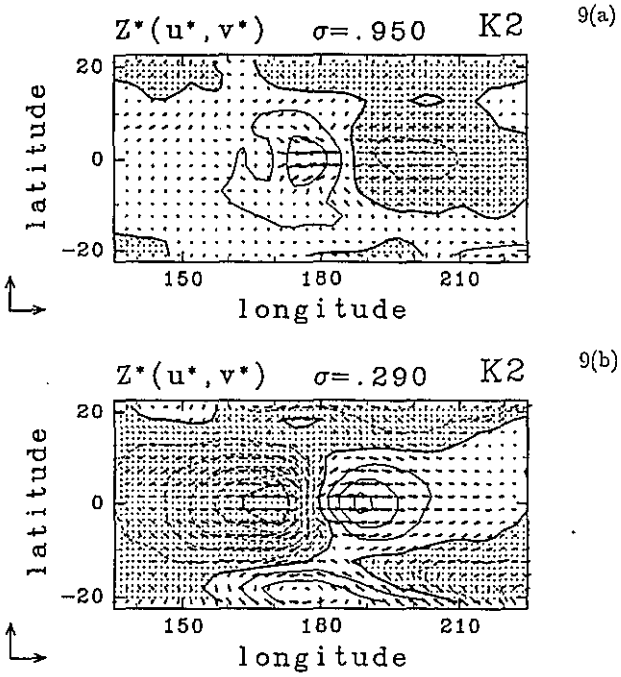

Fig. 9. Longitude–latitude sections of height field equivalent to the field at a constant p surface $Z(\sigma) + g^{-1}RT \ln p_s$ (contour) and wind vectors in composite with reference to precipitation peaks at the equator in experiment K2. Zonal means are subtracted for all quantities. The contour interval is 1 m and negative areas are shaded. The unit vectors shown at the left side bottom represent 5 m/s for both directions. (a) σ =0.95 (about 950 mb), (b) σ=0.29 (about 290 mb).

Figure 10a shows the composite distribution of convergence and horizontal wind in the atmospheric boundary layer around 995 mb. The maximum of convergence is located at about 500 km east of the

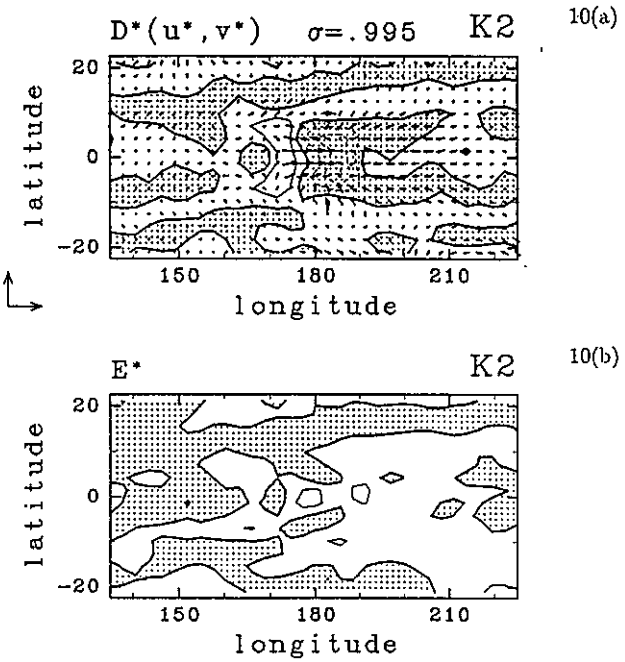

Fig. 10. Horizontal distributions of divergence and evaporation in composite with reference to precipitation peaks at the equator in experiment K2. (a) Divergence (contour) and wind vectors at $\sigma = 0.995$ (about 995 mb). Zonal means are subtracted for all quantities. The contour interval is $1 \times 10^{-6} s^{-1}$ and negative (convergence) areas are shaded. The unit vectors shown at the left side bottom represent 2.5 m/s for both directions. (b) Evaporation from surface. Zonal mean is subtracted. The contour interval is 5 W/m^2 (corresponds to about 0.2 mm/day precipitation) and negative areas are shaded.

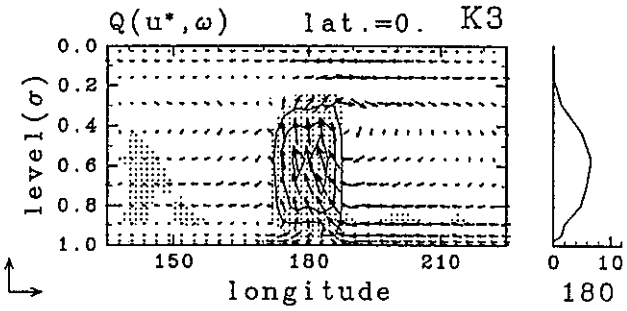

Fig. 11. Longitude–height section of cumulus heating (contour) and wind vectors at the equator in composite with reference to precipitation peaks at the equator in experiment K3. Zonal mean is subtracted for zonal wind. The contour interval is 2K/day and areas of over 1K/day are shaded. Plot on the right side is the vertical distribution of heating (Unit; K/day) at the precipitation peak. The unit vectors shown at the left side bottom represent 5 m/s and 5 mb/hr respectively.

precipitation peak. This maximum seems to be mainly contributed by the zonal convergence caused by the localized westerly wind. The meridional frictional convergence suggested by Wang (1988) does not seem to be significant. The composite distribution of evaporation (Fig. 10b) expresses the tendency that the evaporation is higher to the east of the precipitation peak, although this tendency is not so significant. The local maximum of evaporation is located to the west of the precipitation peak, corresponding to the strong westerly.

4.4 Comparison among three experiments

The composite structure of temperature, wind and cumulus heating fields with reference to precipitation peaks at the equator of experiments K1 and K3 generally look similar to the structure of experiment K2 (Fig. 8). In the vertical profiles of heating there are no significant differences among the three experiments (Fig. 11). However, several characteristic features which appeared in the K2 composite are not so clear in experiment K3, where the coherence of the motion of the areas is not so good. Those are the slantwise phase, the localized downdraft to the west of the precipitation peak and the intense westerly wind near the surface around the peak. On the other hand, there is a region of distinct high temperature and corresponding easterly wind in the low levels to the east of the precipitating area. Note that the wavenumber one structure is dominant in the fields of experiment K3, and the composite may be influenced by such a planetary scale structure.

5. Experiment with moist convective adjustment

In this section, the results of the experiment using the moist convective adjustment scheme as the cumulus parameterization (A1) are described and compared with the results using Kuo's scheme (Sections 3 and 4).

5.1 Latitudinal distribution of precipitation

The latitudinal distribution of zonal and time mean precipitation is shown in Fig. 12. The double ITCZ structure observed in the experiments with Kuo's parameterization (K1∼K3) is not significant in experiment A1. Although there are small peaks at 8 degrees latitudes in both hemispheres, the amount of precipitation is almost uniform from 10 degrees north to 10 degrees south. The precipitation amount at the equator in experiment A1 is larger than that in experiments K1∼K3, whereas the precipitation amount averaged over the entire tropical region shows no significant difference between K1

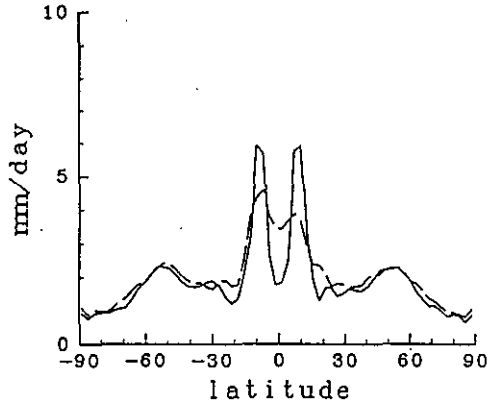

Fig. 12. Latitudinal distributions of time and zonal mean precipitation (Unit; mm/day). Solid line; standard experiment K1. Broken line; experiment with moist convective adjustment A1.

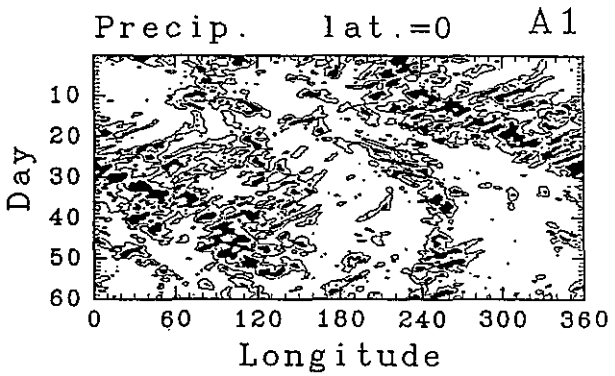

Fig. 13. Longitude-time distribution of precipitation at the equator in experiment A1. Contours indicate 2 mm/day and areas of over 10 mm/day are shaded.

and A1.

5.2 Longitude-time distribution of precipitation at the equator

Figure 13 represents the longitude-time distribution of precipitation at the equator. There are no eastward-moving precipitating areas at the grid scale, as seen in the results of K1∼K3 (Fig. 3). The grid scale precipitation areas rather show westward movement. On the other hand, a remarkable feature of eastward movement is a region of enhanced precipitation with a scale of about 10000 km. It takes about 55 days to encircle the equator, *i.e.*, the speed of propagation is about 8.5 m/s. We refer to this feature an 'eastward-moving planetary scale precipitating region'. The results of the experiment with moist convective adjustment seem greatly different from the results represented by the hierarchical structure of super clusters and the MJ oscillation.

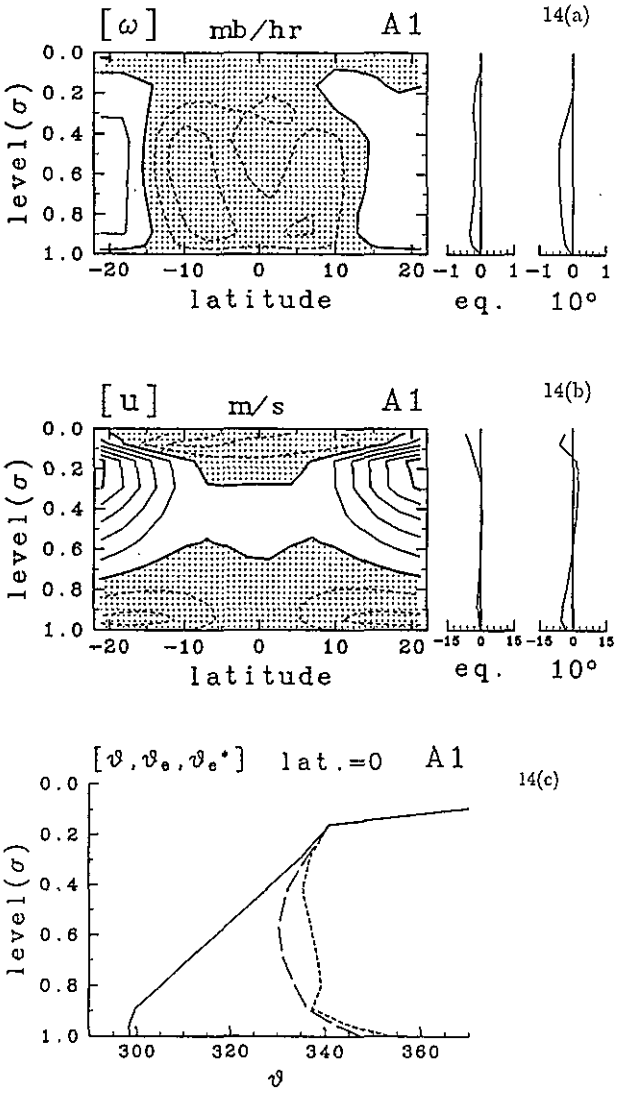

Fig. 14. Zonal and time mean distributions of circulation field in experiment A1. Plots on right side indicate the values at the equator and 10 degrees latitude. (a) Vertical p-velocity [ω]. The contour interval is 0.2 mb/hr and areas of upward motion are shaded. (b) Zonal wind [u]. The contour interval is 3 m/s and negative areas are shaded. (c) Vertical structures of temperature field at the equator in experiment K1 (Unit; K). Solid line; potential temperature. Broken line; equivalent potential temperature. Dotted line; saturated equivalent potential temperature.

5.3 Structure of mean fields

The structures of zonal and time mean fields in experiment A1 are shown in Fig. 14. In experiments K1∼K3, the maximum upward motion is located at 10 degrees latitude and downward motion prevails at the equator. Contrary to these, there is a almost uniform upward motion from 15 degrees north to

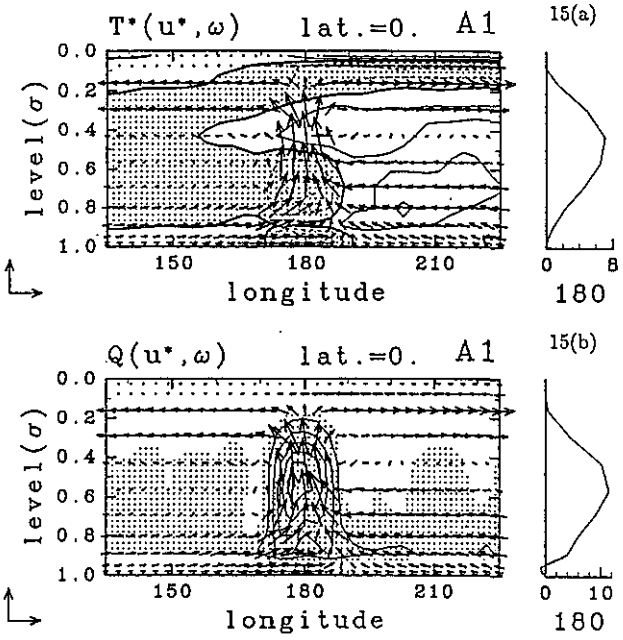

Fig. 15. Composite structures with reference to precipitation peaks at the equator in experiment A1. (a) Longitude–height section of temperature (contour) and wind vectors at the equator. Zonal means are subtracted for temperature and zonal wind. The contour interval is 0.2K and negative areas are shaded. (b) Longitude–height section of heating by cumulus (contour) and wind vectors at the equator. Zonal mean is subtracted for zonal wind. The contour interval is 2K/day and areas of over 1K/day are shaded. Plot on the right side is the vertical distribution of heating (Unit; K/day) at the precipitation peak. In each figure, the unit vectors shown at the left side bottom represent 5 m/s and 5 mb/hr respectively.

15 degrees south in experiment A1, although slight maximum exists around 10 degrees latitude. This corresponds to the uniform latitudinal distribution of precipitation in this region. The zonal wind is almost zero from 10 degrees north to 10 degrees south except for the lower troposphere. This contrasts to the results of experiments K1∼K3, where the state of uniform angular momentum and approximate zero absolute vorticity is realized in the upper troposphere. The angular momentum distribution is not effectively uniformized in experiment A1 because the upward motion is not concentrated at a specific latitude. Figure 14c represents the vertical stratification at the equator. It does not differ much from the result of experiment K1, and qualitatively agrees with the standard stratification of the real tropics (Yanai *et al.*, 1973).

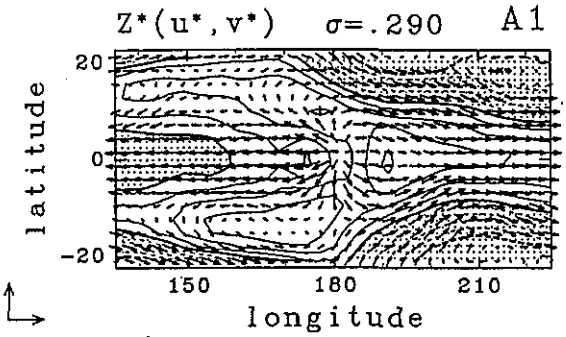

Fig. 16. Longitude–latitude section of height field equivalent to the field at a constant p surface $Z(\sigma) + g^{-1}RT\ln p_s$ (contour) and wind vectors at $\sigma=0.29$ in composite with reference to precipitation peaks at the equator in experiment A1. Zonal means are subtracted for all quantities. The contour interval is 1 m and negative areas are shaded. The unit vectors shown at the left side bottom represent 5 m/s for both directions.

5.4 Structure of circulations associated with grid scale precipitating areas at the equator

The composite structures of the grid scale precipitating areas of experiment A1 (Fig. 15) show a very different nature from that of experiments K1∼K3. The westward slant of the phase line is not clearly observed, except at the lowest levels ($\sigma \geq 0.9$) where the updraft is stronger to the east of the precipitation peak. The specific feature not observed in experiments K1∼K3 is the region of cold temperature under the 900 mb level over the precipitating area. This is formed by low level cooling with the moist convective adjustment, which appears in the vertical distribution of heating (Fig. 15b). There is a high temperature region to the east of the peak and a low temperature region to the west in general, which reflects the planetary scale structure rather than the structure associated with the grid scale precipitating area. Over the precipitation peak, the upper layer around 400 mb level has a warm anomaly and the lower layer around 700 mb level has a cold anomaly. The amplitude of circulation in experiment A1 is somewhat stronger than that in experiments K1∼K3.

Figure 16 represents the horizontal structure in the upper troposphere. Existence of vortices to the west of the precipitation peak is clear. This structure much resembles Gill (1980)'s pattern, which the results of experiments K1∼K3 do not show. This is consistent with the fact that the mean zonal wind field is quite different from those in the experiments K1∼K3.

6. Discussion

The precipitating area which is called the 'super cluster' by HS86, is found to be represented in the model as a grid scale precipitation area which moves eastward continuously and accompanies a distinct structure of circulation. However, this structure appears only in the experiments using Kuo's parameterization. The behavior of precipitation is quite different when the moist convective adjustment scheme is used. Based on those results, we will try to discuss the origin and the causes of the parameter dependence of the structures.

6.1 Structure of the circulation associated with the grid scale precipitation areas

Firstly, we will consider the eastward-moving precipitating areas at the equator shown in the experiments with Kuo's parameterization and the structure of circulation associated with them.

The remarkable features of the circulation with eastward-moving precipitating areas on the grid scale are summarized as follows;

(1) resemblance to the Kelvin wave, *i.e.*, the dominance of zonal wind and in-phase relationship between zonal wind and height,

(2) localized downdraft to the west of the precipitation peak,

(3) intense westerly wind at low levels just over the precipitation peak,

(4) large difference in structure between the upper troposphere and the lower troposphere.

As for a response of the tropical atmosphere to a heat source, the steady linear response calculated by Gill (1980) is well known. It is often assumed that the 'first baroclinic mode'[3] dominates in the response to heatings with a maximum in the middle troposphere. However, it is difficult to describe the structure associated with the precipitating area in the model by use of the 'first baroclinic' response only. Our results show that the structure should be considered to be a superposition of the 'first baroclinic mode' circulation and those of shorter vertical wavelengths. In Fig. 8, the 'first baroclinic mode' appears as the structure with an updraft at 180 degrees and high (low) temperature to the east (west). The 'second baroclinic mode' also appears as the structure with a downdraft at around 170 degrees and a high (low) temperature to the west (east) in the lower layer, and with an updraft and the reverse temperature structure in the upper layer.

[3]We use this word conventionally, although such a mode is not actually the first of the calculated vertical normal modes.

It is shown in the Appendix that such a structure is represented as a linear response to a moving and growing heat source confined spatially. It is also demonstrated that the solution in which the motion and growth of the given heat source is consistent with the phase propagation and growth of the induced circulation corresponds to a linear wave-CISK mode. There are several factors included in GCMs that cannot be expressed in the simple model in the Appendix, such as nonlinearity, dissipation and vertical shear. Regardless of these factors, this linear response reproduces well the characteristic features of the circulation associated with the precipitating area, especially item (2) and (3) listed above.

Judging from the structure seen in Fig. 10, it is difficult to accept that the frictional CISK mechanism of Wang (1988) or evaporation-wind feedback mechanism of Emanuel (1987) is effective for the maintenance of the grid scale precipitating areas. This notion will be confirmed in part II (Numaguti and Hayashi, 1991). On the other hand, the structure associated with the grid scale precipitating area has a characteristic feature of modal solutions obtained by the linear wave-CISK theory. Thus, the grid scale precipitating area is considered to be maintained by the wave-CISK mechanism. It is plausible that the dominance of the small scale comes from the nature of wave-CISK: The growth rate of the smallest scale is maximum for Kelvin wave modes in the linear theories.

The difference of structure between the upper and the lower layers can be attributed to the difference of the mean vorticity fields. Since the gradient of mean absolute vorticity is small in the upper levels, a heat source excites pure gravity waves, whereas it excites Kelvin waves at lower levels.

HS86 states that the eastward-moving disturbances at the equator in their model can be interpreted as a mode in which the Kelvin wave and the Rossby wave are coupled together. Furthermore, Chao (1987) suggests the importance of Rossby mode response in the context of a linear response to a moving heat source. However, from our analyses, any significant contribution of the structures characterized by the nature of Rossby wave is not observed in the structure of super cluster in the model.

6.2 Speed of eastward movement and its dependence on SST

It is well known that the vertical profile of heating is an important factor for the propagation speed of modes in the linear theory of wave-CISK (Takahashi, 1987). Generally, it is believed that the propagation speed becomes higher when the peak of the heating is higher (Tokioka *et al.*, 1988).

Our experiments K1$\sim$K3 showed that the speed of movement of precipitating areas is higher with higher SST. However, in the vertical profile of heat-

ing there seems to be no significant difference between K2 (Fig. 8c) and K3 (Fig. 11). What must be taken into account for the discussion of the propagation speed in addition to the vertical profile of heating is the state of stratification. The distributions of static stability N^2 in Fig. 6 show significant differences among the three experiments, especially in the upper troposphere. The static stability in experiment K2 is about 1.4 times larger than that of experiment K3, which corresponds to a difference of a phase velocity of factor 1.2. This difference may be the principal factor of the difference of the eastward moving speed (factor 1.3) in the model.

In the results of Swinbank *et al.* (1988), the propagation speed of a planetary scale disturbance is reduced by an increase of SST or efficiency of heating. They interpreted this reduction of speed as an enhancement of the 'reduced gravity effect' (Gill, 1982). However, our results are opposite and do not support their interpretation. In the framework of linear theory, the speed of the 'first baroclinic mode' is indeed slowed down by an increase of heating. However, we have to notice that the speed of the 'second baroclinic mode' is actually accelerated by the same increase ('enhanced stability effect'). Hence, it is unclear whether the wave-CISK mode, which is the coupling of the first and second baroclinic modes, propagates faster or not. It is not clear where the difference between our results and Swinbank *et al.* (1988)'s comes from. From our results, it is suggested that the change of the stratification must not be neglected.

6.3 Dependence of the behavior of precipitating areas on cumulus parameterization

In the experiment with the moist convective adjustment scheme A1, the behavior of precipitation is qualitatively different from the results of K1$\sim$K3, and the 'super cluster' does not exist. This suggests that the mechanism of wave-CISK is not effective on the grid scale when the moist convective adjustment is used.

The first candidate of the cause of the difference is the difference of the switching condition of the parameterizations. Kuo's scheme explicitly requires a moisture convergence as a switching condition, while the moist adjustment scheme does not require a moisture convergence explicitly. One may speculate that Kuo's scheme is closer to the parameterization which is utilized in the linear theories of wave-CISK in this sense. Further analysis of the model results (not shown) suggests that the most critical condition of switching in Kuo's scheme is indeed the existence of moisture convergence. On the other hand, when the moist convective adjustment scheme is used, it is the relative humidity at the middle levels that controls the switching of the parameterization. The change of the stratification is not a very important factor of switching of the adjustment scheme, because the stratification is almost always neutral or rather unstable in the model tropical atmosphere. The important fact is that moisture convergence should occur for the relative humidity at middle levels to be sufficiently high, which means that the adjustment scheme *implicitly* requires a moisture convergence as a switching condition. Therefore, it is premature to conclude that the Kuo's scheme is more effective for wave-CISK than the moist convective adjustment scheme simply from the apparent difference of switching conditions of the parameterizations.

The next factor to be considered is the vertical profile of heating. Simple linear theory suggests that some conditions in vertical profile must be satisfied for a heating to promote wave-CISK modes. In the composite figures (Fig. 8c, Fig. 15b), though the absolute strength of the heating is somewhat different, the vertical profiles of heating of A1 and K2 are very similar except for the lowest levels. The moist convective adjustment tends to cool the lowest levels, which may hinder the endurance of precipitation in experiment A1 to some extent.

The third factor, which must be stressed here, is the representativeness of the composite heatings. In experiments K1$\sim$K3, the representativeness of the composite figure is fairly good, whereas it is questionable in experiment A1. Figure 17 compares the composite and snapshot distributions of cumulus heating and vertical velocity in experiments K2 and A1. In experiment K2, the snapshot distributions (Fig. 17c) correlate quite well with the composite distributions (Fig. 17a), and the heating profile is almost constant in time. In experiment A1, on the other hand, the snapshots do not always resemble the composite charts, and the variability of heating profile is large. Moreover, contrary to the composite structure, the phases of updraft and heating are the same everywhere in the snapshot. As stated in the introduction, the heating which has such a phase relationship with the circulation cannot maintain a propagating wave-CISK mode. This difference of the heating of two parameterization schemes is considered to be caused by the characteristics of the schemes. In the Kuo scheme, the coupling between the upper layer and the lower layer is strong because the heating extends to the upper layer whenever the lower layer satisfies the condition of convection. In the moist convective adjustment scheme, on the other hand, the heating occurs independently between layers because the condition for convection of each layer is judged without referring the condition of the other layers. It is considered that the difference of the behavior of grid scale precipitating areas is caused by the difference of effectiveness of wave-CISK mechanism which is controled by the vertical coherence of the heating. Unfortunately, the infor-

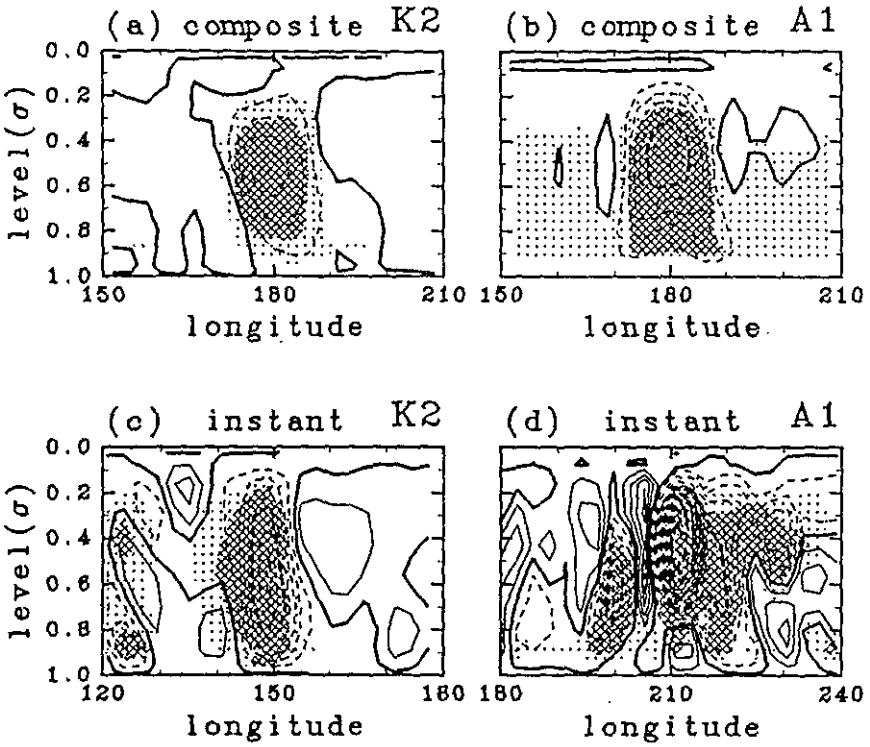

Fig. 17. Longitude–height distributions of cumulus heating (tone) and vertical motion (contour) at the equator in experiment K2 and A1. Light tone denotes areas of over 1K/day and dark tone denotes areas of over 3K/day. The contour interval is 1 mb/hr and negative contours are drawn in broken line. (a) Composite in experiment K2, (b) composite in experiment A1, (c) snapshot in experiment K2, (d) snapshot in experiment A1.

mation about the time-space distribution of heating in the real atmosphere, especially on the vertical profile, is so scant that we cannot judge which parameterization is superior in simulating the real atmosphere.

7. Conclusions

The hierarchical structures of cumulus activity reported in HS86, *i.e.*, the super cluster, the 30-day oscillation and double ITCZs, and their parameter dependence are examined through GCM experiments.

The following results are obtained from the experiments with Kuo's cumulus parameterization and various values of SST:

(1) The double ITCZ structure clearly appears in all the three experiments, especially in the experiment with the high SST value.

(2) The 'super cluster' shown by HS86 is expressed in the model as an eastward-moving precipitating area on the grid scale.

(3) The activity of the eastward-moving precipitating areas of the grid scale has an exclusive relation with the activity of the planetary scale modulation structure. The former is active in the high SST experiment, whereas the latter is distinct in the low SST experiment.

(4) A specific circulation structure is associated with the eastward-moving precipitating areas. This structure is dynamically consistent as a response to the eastward-moving and growing heat source. It is considered to be maintained by the wave-CISK mechanism of Kelvin waves.

(5) The speed of the movement of the structure associated with the grid scale precipitating areas is faster under the condition of the higher SST. This dependence is partly explained by the change of the static stability, which is approximately determined by the moist adiabatic lapse rate. The factor of variation of the stratification is not negligible in the discussion of propagation speed.

An experiment with the moist convective adjustment scheme is performed and compared with the results of the experiments with Kuo's parameterization.

(6) The separation of the ITCZ into double bands is not clear in the experiment with

moist convective adjustment.

(7) The dependence of the behavior of grid scale precipitating areas on cumulus parameterizations is fairly large. In the experiment with the moist convective adjustment, there is no continuous eastward movement of grid scale precipitating areas, whereas an eastward-moving planetary scale structure is clearly observed.

(8) In the experiment with Kuo's parameterization, the propagating wave-CISK mechanism works effectively because the convergence field at lower levels controls the heating in the whole troposphere above. On the other hand, the moist convective adjustment scheme has characteristics that the heating of each layer is determined independently and the vertical coupling is weak, so that the propagating grid scale structure cannot be maintained by the wave-CISK.

An important issue which remains still unclear is whether the 'super cluster' of Nakazawa (1988) is comparable to the model 'super cluster', *i.e.* the eastward-moving precipitating area on grid scale. Since the horizontal scale of the grid scale precipitating areas in the model is near the smallest resolvable scale, it is questionable whether this feature holds a physical reality. However, the result of the model clarified that they associate the circulations whose characteristics are easy to be understood dynamically. It is not considered that they are mere computational noises. It seems that there is no definitive difference between the structure of grid scale precipitating areas in the model and the structure of the real super clusters shown in Nakazawa (1988). However, the comparison is far from conclusive, since the results with the convective adjustment scheme are quite different from those with Kuo's scheme. In order to make a further discussion on the correspondence between the model result and the real atmosphere, the problem of parameterization dependence must be overcome. Experiments with increased resolution are also highly desirable.

In Part II of this study, an analysis of the results of the same experiments are performed concentrating on the planetary scale structure and the structure of precipitating areas around the ITCZ latitudes in order to discuss the origin of the hierarchical structure of cumulus activity.

Acknowledgements

The authors would like to thank Profs. T. Matsuno and A. Sumi for valuable discussions and encouragement, and Mr. N. Sato of the Japan Meteorological Agency for providing the original model code. Comments by Prof. K. Emanuel and anonymous reviewers are helpful to improve the original manuscript. Discussions with Dr. K. Masuda and Mr. K. Nakajima were also helpful. This research was supported by Grant-in-Aid, Ministry of Education, Science and Culture. The computation was made on HITAC-S820 and M-680H computers of the Computer Center, University of Tokyo. For drawing the figures, the GFD–DENNOU Library produced by Drs. M. Shiotani and S. Sakai was used.

Appendix

A linear model of responses to heating

In this appendix, responses to a moving and growing heating are examined using a two-dimensional linear model.

The characteristics of a Kelvin wave on an equatorial β plane can be illustrated in the two-dimensional framework of longitude and height, so long as the meridional structure and the effect of friction are not concerned:

$$\frac{\partial u}{\partial t} = -\frac{\partial \phi}{\partial x} , \tag{4}$$

$$\frac{\partial}{\partial t}\frac{\partial \phi}{\partial z} + N^2 w = Q , \tag{5}$$

$$\frac{\partial u}{\partial x} + \frac{1}{p}\frac{\partial pw}{\partial z} = 0 . \tag{6}$$

Here, u is zonal wind, w vertical wind, ϕ geopotential, Q heat source and p is pressure. t, x are the time and longitudinal coordinate respectively. The $\log p$ coordinate z is defined as:

$$z \equiv -H \log \frac{p}{p_0} , \tag{7}$$

$$H \equiv \frac{RT_0}{g} , \tag{8}$$

where T_0 is the representative temperature, R gas constant, and g is acceleration gravity. N^2 is the vertical static stability defined as:

$$N^2(z) \equiv \frac{R}{H}\frac{d\bar{T}}{dz} + \frac{g^2}{C_p T_0} , \tag{9}$$

where $\bar{T}$ is temperature of basic state and C_p is specific heat of air.

As the boundary condition, the rigid lid conditions are applied at $z=0$ and $z=D$ for simplicity.

$$w = 0 \quad \text{at } z = 0, D . \tag{10}$$

The periodic boundary condition is applied to the longitudinal direction.

$$u(x, z) = u(x + 2\pi L, z) \quad etc. \tag{11}$$

where $2\pi L$ is the longitudinal circumference. The static stability N^2 is assumed to be a constant independent of z.

The following form of heat source is assumed:

$$Q(x,z,t) = \eta(z)\tilde{Q}(x-Ct)\ , \tag{12}$$

which means that the heat source is moving at a speed of $C_r = \mathcal{R}e\, C$. Note that we will retain C as a given complex value; $C \equiv C_r + iC_i$.

The solutions are expanded into the vertical normal modes of $Q=0$. Thus the equations are separated into the vertical structure equation,

$$\frac{d}{dz}\left(\frac{1}{p}\frac{d}{dz}pW_n(z)\right) = -\frac{1}{{C_n}^2}N^2W_n(z)\ , \tag{13}$$

and the horizontal structure equations,

$$\frac{\partial}{\partial t}\tilde{u}_n = -\frac{\partial}{\partial x}\tilde{\phi}_n\ , \tag{14}$$

$$\frac{\partial}{\partial t}\tilde{\phi}_n + {C_n}^2\frac{\partial}{\partial x}\tilde{u}_n = -{C_n}^2\eta_n\tilde{Q}(x-Ct)\ . \tag{15}$$

Here, C_n is the propagation velocity of the n-th free mode. η_n is the coefficient in expansion of $\eta(z)$ of the following form:

$$\eta(z) = \sum_{n=1}^{\infty}\eta_n W_n(z)N^2\ . \tag{16}$$

The solution of vertical structure equation is obtained by the use of boundary conditions as:

$$W_n(z) = \sin\left(\frac{n\pi}{D}z\right)\exp\left(-\frac{z}{2H_0}\right)\ , \tag{17}$$

$$C_n = N\left[\left(\frac{n\pi}{D}\right)^2 + \frac{1}{4H^2}\right]^{-1/2}\ . \tag{18}$$

The response is obtained easily from the horizontal structure Eqs. (12) and (13). The solution has both eastward-propagating modes and westward-propagating modes. However, taking account for the correspondence to Kelvin wave, the solution composed of only eastward-propagating modes is accounted in the following. The response of w is given by:

$$w(x,z,t) = \sum_n \frac{{C_n}^2\eta_n}{{C_n}^2 - (C_r+iC_i)^2}W_n(z)\tilde{Q}(x-Ct)\ , \tag{19}$$

and the response for other variables can be obtained in the similar manner. In the following, all variables are expressed in nondimensional form, using the scales $(L, D, NL/D)$ for (x,z,t).

Assume that the heat source can be expanded into sinusoidal waves of the form:

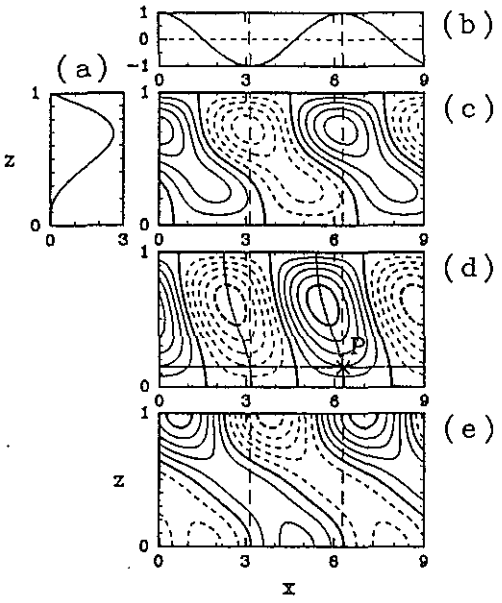

Fig. A1. Responses to a moving and growing heat source in the linear model. The case of the longitudinally sinusoidal heating with two vertical modes. The value of normalized parameters are $C_r=0.062$ and $C_i=0.031$. Phase speed of $n=1$ mode is 0.1 and that of $n=2$ mode is 0.05 in this unit. (a) Vertical distribution of heating $\eta(z)$, (b) horizontal distribution of heating $\tilde{Q}(x)$, (c) temperature T, (d) vertical velocity w, (e) zonal velocity u.

$$\tilde{Q}(x-Ct) = \sum_k Q_k \exp[ik(x-C_rt) + kC_it]\ . \tag{20}$$

This expresses the heating which is moving at the speed C_r and growing at the growth rate kC_i. The response is obtained by summing up the response for each longitudinal mode k.

Assume the vertical profile of heating as shown in Fig. A1a. This profile is the superposition of two vertical normal mode $n=1$ and $n=2$. Figs. A1c–A1e show the responses to the heating with only one wave component in longitudinal direction (Fig. A1b). The structure shows a slantwise character because the amount of longitudinal phase shift is different from mode to mode. When the heating has only one vertical mode, the slantwise character does not appear as shown in Fig. A2 and Fig. A3.

Let us introduce a parameterization in which the heating is determined to be proportional to the vertical velocity at a certain level of the lower 'troposphere'. The circulation response in which the phase of this parameterized heating coincides with the initially given heating can be regarded as a wave-CISK mode. For the case of the vertical profile of heating given in Fig. A1a, Fig. A1d exhibits that the phase of the initially given heating coincides with the ver-

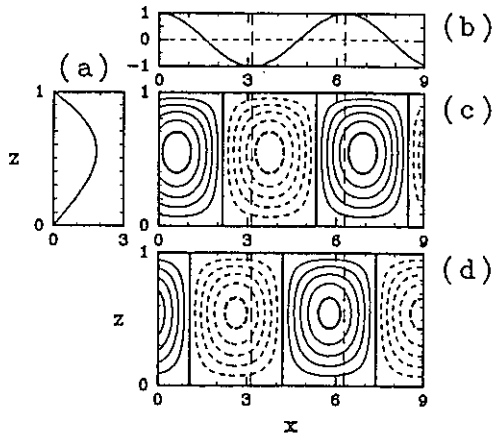

Fig. A2. Responses to a moving and growing heat source in the linear model. The case of the longitudinally sinusoidal heating with only one vertical mode $n=1$. $C_r=0.062$ and $C_i=0.031$. (a) Vertical distribution of heating $\eta(z)$, (b) horizontal distribution of heating $\tilde{Q}(x)$, (c) temperature T, (d) vertical velocity w.

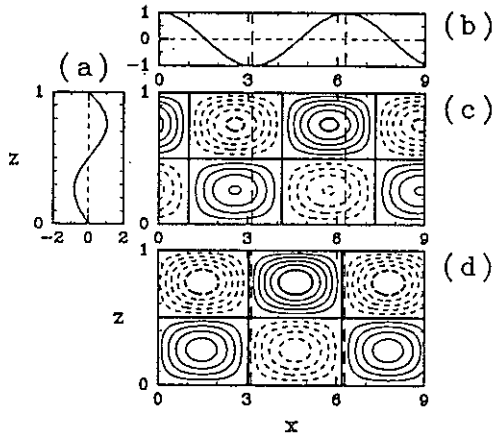

Fig. A3. Responses to a moving and growing heat source in the linear model. The case of the longitudinally sinusoidal heating with only one vertical mode $n=2$. $C_r=0.062$ and $C_i=0.031$. (a) Vertical distribution of heating $\eta(z)$, (b) horizontal distribution of heating $\tilde{Q}(x)$, (c) temperature T, (d) vertical velocity w.

tical velocity at the level indicated in the figure. At the point P in Fig. A1d, for instance, the broken lines which denote the maximum–minimum phase of the given heating crosses the dotted lines which denote the maximum–minimum phase of the vertical velocity. Therefore, if the reference level used in the parameterization is chosen to be the level which includes the point P, the structure shown in Fig. A1c–A1e can be regarded as a wave-CISK mode. For the case of the vertical profile of heating given in Fig.

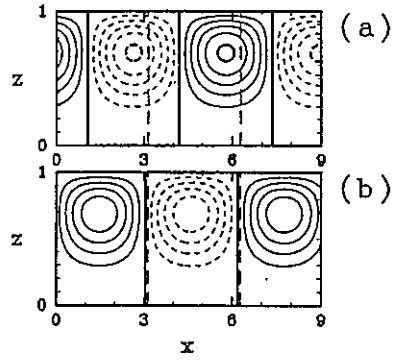

Fig. A4. Heating distributions parameterized by the low level vertical velocity of the response of each mode (Fig. A2 and A3). (a) Heating parameterized by $n=1$ mode circulation, (b) heating parameterized by $n=2$ mode circulation.

A2a or Fig. A3a, which is composed of only one vertical mode, Figs. A2 or Figs. A3 indicates that the phase of initially given heating never coincides with that of the vertical velocity of a response to a moving and growing heating. The structures shown in Figs. A2 and Figs. A3 cannot form wave-CISK modes by themselves.

The structure shown in Fig. A1, which can be regarded as a wave-CISK mode, can be described in terms of the interaction of two vertical modes. Figs. A2 and Figs. A3 are actually the vertical decomposition of the given heating and the response fields of Figs. A1. The parameterized heating mentioned above can be horizontally decomposed into the following two parts. One is the portion which is proportional to the vertical velocity at the reference level associated with mode $n=1$ (Fig. A2d). This is expressed in Fig. A4a and called 'heating parameterized by $n=1$ mode circulation'. The other is the portion which is proportional to the vertical velocity at the same level but with mode $n=2$ (Fig. A3d), which is expressed in Fig. A4b and called 'heating parameterized by $n=2$ mode circulation'. Note that the vertical profile of thus decomposed heating are the same one given in Fig. A1a, which include both of the vertical modes. Now, let us trace the way in which the decomposed heatings affect the circulation of the other modes. The heating parameterized by $n=1$ mode circulation (Fig. A4a) positively correlates with the temperature distribution of the $n=2$ mode (Fig. A3c). Similarly, the heating parameterized by the $n=2$ mode circulation (Fig. A4b) positively correlates with temperature distribution of the $n=1$ mode (Fig. A2c). Thus the growth of modes is realized by mutual enhancement through the heating. In this situation, wave-CISK modes exist only if the signs of the $n=1$ vertical component and $n=2$ vertical component of the heating are opposite in the reference level of parameterization,

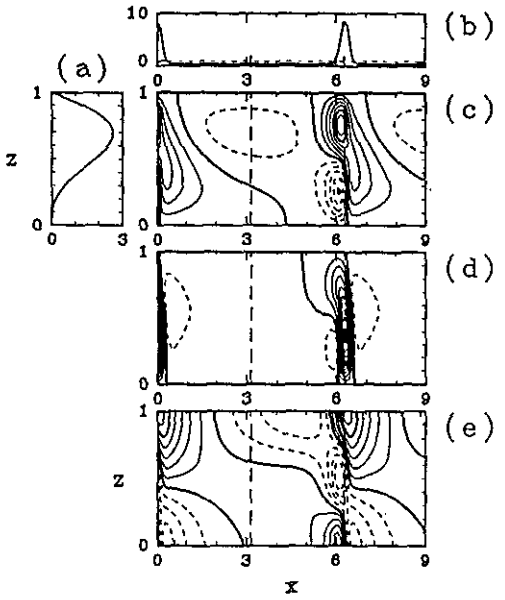

Fig. A5. Responses to a moving and growing heat source in the linear model. The case of the longitudinally Gaussian heating with two vertical modes. $C_r=0.062$ and $C_i=0.031$. (a) Vertical distribution of heating $\eta(z)$, (b) horizontal distribution of heating $\tilde{Q}(x)$, (c) temperature T, (d) vertical velocity w, (e) zonal velocity u.

that is, the heating is more intense in the upper levels than in the lower levels. If it is not the case, two modes cannot enhance each other. When the phase relationship is such that the heating parameterized by $n=1$ mode circulation act to enhance the $n=2$ mode circulation, the heating parameterized by $n=2$ mode circulation acts to weaken the $n=1$ mode circulation. And when the phase relationship is opposite, the heating parameterized by the $n=1$ mode circulation act to weaken the $n=2$ mode circulation.

In the structure accompanied by the grid scale precipitating areas in the GCM, the heating and the updraft are confined locally. In order to demonstrate this feature with a linear model, a response to a confined heating is examined by superposing heatings of various longitudinal wavenumbers. Figs. A5 show the response to a heating of a Gaussian shape. There is a longitudinally confined updraft with a slantwise structure. To the west of the updraft, a localized downdraft emerges in the lower levels. Moreover, an intense westerly wind just below the heating appears. These are the characteristics seen in the composite of eastward-moving precipitating areas of the grid scale in GCM. The response of the $n=2$ mode is important in reproducing such a characteristic structure.

References

Bolton, D., 1980: Application of the Miles theorem to forced linear perturbations. *J. Atmos. Sci.*, **37**, 1639–1642.

Chang, C.-P. and H. Lim, 1988: Kelvin wave-CISK: A possible mechanism for the 30–50 day oscillations. *J. Atmos. Sci.*, **45**, 1709–1720.

Chao, W.C., 1987: On the origin of the tropical intraseasonal oscillation. *J. Atmos. Sci.*, **44**, 1940–1949.

Charney, J.G. and A. Eliassen, 1964: On the growth of the hurricane depression. *J. Atmos. Sci.*, **21**, 68–75.

Emanuel, K.A., 1986: An air-sea interaction theory for tropical cyclones. Part I: Steady-state maintenance. *J. Atmos. Sci.*, **43**, 585–604.

Emanuel, K.A., 1987: An air-sea interaction model of intraseasonal oscillations in the tropics. *J. Atmos. Sci.*, **44**, 2324–2340.

Gill, A.E., 1980: Some simple solutions for heat-induced tropical circulation. *Quart. J. Roy. Meteor. Soc.*, **106**, 447–462.

Gill, A.E., 1982: Studies of moisture effects in simple atmospheric models: the stable case. *Geophys. Astrophys. Fluid Dyn.*, **19**, 119–152.

Hayashi, Y., 1970: A theory of large-scale equatorial waves generated by condensation heat and accelerating the zonal wind. *J. Meteor. Soc. Japan*, **48**, 140–160.

Hayashi, Y.-Y. and T. Nakazawa, 1989: Evidence of the existence and eastward motion of superclusters at the equator. *Mon. Wea. Rev.*, **117**, 236–243.

Hayashi, Y.-Y. and A. Sumi, 1986: The 30–40 day oscillations simulated in an "aqua planet" model. *J. Meteor. Soc. Japan*, **64**, 451–467.

Held, I.M. and A.Y. Hou, 1980: Nonlinear axially symmetric circulations in a nearly inviscid atmosphere. *J. Atmos. Sci.*, **37**, 515–533.

Hubert, L.F., A.F. Krueger and J.S. Winston, 1969: The double intertropical convergence zone—fact or fiction? *J. Atmos. Sci.*, **26**, 771–773.

Kanamitsu, M., K. Tada , T. Kudo, N. Sato and S. Isa, 1983: Description of the JMA operational spectral model. *J. Meteor. Soc. Japan*, **61**, 812–827.

Katayama, A., 1972: A simplified scheme for computating radiative transfer in the troposphere. Numerical Simulation of Weather and Climate. *Tech. Rept.*, No. 6, Univ. California Los Angels, 77 pp.

Kuo, H.L., 1974: Further studies of the parameterization of the influence of cumulus convection on large-scale flow. *J. Atmos. Sci.*, **34**, 1232–1240.

Lau, K.-M. and L. Peng, 1987: Origin of low-frequency (intraseasonal) oscillations in the tropical atmosphere. Part I: Basic theory. *J. Atmos. Sci.*, **44**, 950–972.

Lau, N.-C., I.M. Held and J.D. Neelin, 1988: The Madden-Julian oscillation in an idealized general circulation model. *J. Atmos. Sci.*, **45**, 3810–3832.

Lindzen, R.S., 1974: Wave-CISK in the tropics. *J. Atmos. Sci.*, **31**, 156–179.

Madden, R.A. and P.R. Julian, 1972: Description of global-scale circulation cells in the tropics with 40–50 day period. *J. Atmos. Sci.*, **29**, 1109–1123.

Manabe, S., J. Smagorinsky and R.F. Strickler, 1965: Simulated climatology of a general circulation model with a hydrologic cycle. *Mon. Wea. Rev.*, **93**, 769–798.

Murakami, T., T. Nakazawa and J. He, 1984: On the 40–50 day oscillations during the 1979 northern hemisphere summer. Part I: Phase propagation. *J. Meteor. Soc. Japan*, **62**, 440–468.

Nakazawa, T., 1988: Tropical super clusters within intraseasonal variations over the western Pacific. *J. Meteor. Soc. Japan*, **66**, 823–839.

Neelin, J.D., I.M. Held and K.H. Cook, 1987: Evaporation-wind feedback and low-frequency variability in the tropical atmosphere. *J. Atmos. Sci.*, **44**, 2341–2348.

Numaguti, A. and Y.-Y. Hayashi, 1991b: Behaviors of cumulus activity and the structures of circulations in an "aqua planet" model. Part II: Eastward moving planetary scale structure and the intertropical convergence zone. *J. Meteor. Soc. Japan*, **69**, 563–579.

Ose, T., T. Tokioka and K. Yamazaki, 1989: Hadley circulations and penetrative cumulus convection. *J. Meteor. Soc. Japan*, **67**, 605–619.

Reed, R.J. and E.E. Recker, 1971: Structure and properties of synoptic-scale wave disturbances in the equatorial western Pacific. *J. Atmos. Sci.*, **28**, 1117–1133.

Swinbank, R., T.N. Palmer and M.K. Davey, 1988: Numerical simulations of the Madden and Julian oscillation. *J. Atmos. Sci.*, **45**, 774–788.

Takahashi, M., 1987: A theory of the slow phase speed of the intraseasonal oscillation using the wave-CISK. *J. Meteor. Soc. Japan*, **65**, 43–49.

Tokioka, T., K. Yamazaki, A. Kitoh and T. Ose, 1988: The equatorial 30–60 day oscillation and the Arakawa-Schubert penetrative cumulus parameterization. *J. Meteor. Soc. Japan*, **66**, 883–901.

Wang, B., 1988: Dynamics of tropical low-frequency waves: An analysis of the moist Kelvin wave. *J. Atmos. Sci.*, **45**, 2051–2065.

Xu, K.-M. and K.A. Emanuel, 1989: Is the tropical atmosphere conditionally unstable? *Mon. Wea. Rev.*, **117**, 1471–1479.

Yanai, M., S. Esbensen and J.-H. Chu, 1973: Determination of bulk properties of tropical cloud clusters from large-scale heat and moisture budgets. *J. Atmos. Sci.*, **30**, 611–627.

Zangvil, A., 1975: Temporal and spatial behavior of large-scale disturbances in tropical cloudiness deduced from satellite brightness data. *Mon. Wea. Rev.*, **103**, 904–920.

「水惑星」モデルにおける熱帯域の積雲活動のふるまいと循環構造
第1部　スーパークラスターの構造

沼口　敦・林　祥介
（東京大学理学部地球惑星物理学教室）

Hayashi and Sumi (1986, HS86) による「水惑星モデル」実験の続きとして、下部境界条件として与える海面温度を変化させたモデル実験ならびに積雲パラメタリゼーションを換えたモデル実験を行なった。HS86で指摘された積雲活動の特徴的な分布のパラメータ依存性と、それにともなう循環の構造を調べた。第1部では主にスーパークラスターについての記述を行なう。

HS86の実験で現れたスーパークラスターは、モデル上においては赤道付近における格子点スケールの降水域の持続的な東進として現れる。それにともなう循環の構造は、基本的にKelvin波のwave-CISKの力学によって説明されうる。スーパークラスターは海面水温を上げることによって活発化するが、30日振動すなわち惑星スケールの東進構造は海面水温が低い場合において顕著となる。

格子点スケールの積雲活動域のふるまいは、積雲パラメタリゼーションの違いに敏感である。Kuoのパラメタリゼーションのかわりに湿潤対流調節を用いると赤道上での格子点スケールでの持続的な東進構造は現れなくなる。それに対して惑星スケールの構造は湿潤対流調節を用いた場合でも顕著である。